Fluid Dynamics Research

The Japan Society of Fluid Mechanics

PAPER

Effect of hydrodynamic slippage on electro-osmotic flow in zeta potential patterned nanochannels

To cite this article: S Datta and J N Choudhary 2013 *Fluid Dyn. Res.* **45** 055502

View the article online for updates and enhancements.

Related content

- Electro-osmotic flow through a thin channel with gradually varying wall potential and hydrodynamic slippage
Chiu-On Ng and Qi Zhou
- Electro-osmotic dispersion in a circular tube with slipstick striped wall
Qi Zhou and Chiu-On Ng
- Oscillatory electro-osmotic flow through a slit channel with slipping stripes on walls
Henry C W Chu and Chiu-On Ng

Recent citations

- Electroosmotic flow in a slit nanochannel with superhydrophobic walls
Simanta De *et al*
- Electro-osmotic dispersion in a circular tube with slip-stick striped wall
Qi Zhou and Chiu-On Ng

This content was downloaded from IP address 103.27.9.249 on 31/12/2017 at 05:55

IOP PUBLISHING FLUID *DYNAMICS* RESEARCH

Fluid Dyn. Res. **45** (2013) 055502 (14pp) doi:10.1088/0169-5983/45/5/055502

Effect of hydrodynamic slippage on electro-osmotic flow in zeta potential patterned nanochannels

S Datta and J N Choudhary

Department of Mechanical Engineering, Indian Institute of Technology Delhi, Hauz Khas, New Delhi 110016, India

E-mail: subhra-datta@iitd.ac.in

Received 13 January 2013, in final form 15 June 2013
Published 5 August 2013
Online at stacks.iop.org/FDR/45/055502

Communicated by M Maxey

Abstract

The effect of hydrodynamic slippage on the electro-osmotic flow in a nanochannel with thick electrical double layers whose wall surface potential has a periodic axial variation is studied. The equations of Stokes flow are solved exactly with the help of the Navier slip boundary condition and the Debye–Huckel linearization of the equation governing the potential of the electrical double layer. Each periodic cell of the flow field consists of four counter-rotating vortices. The cross-channel profile of the axial velocity at the center of the cell exhibits three extrema and a reversed velocity zone near the channel axis of symmetry. The size of the extrema and that of the reversed velocity zone increases with increase in the degree of slippage. In the limit when the wavelength of axial variation in surface potential is much larger than the channel width, the flow characteristics are interpreted in terms of the lubrication approximation. In the limit when the electrical double layer is much thinner than the channel height, the effect of slip is modeled by a Helmholtz–Smoluchowski apparent slip boundary condition that depends on the pattern wavelength.

(Some figures may appear in colour only in the online journal)

1. Introduction

Electro-osmotic flow has emerged as a popular alternative to pressure-driven flow in microfluidic applications (Stone *et al* 2004). Electro-osmotic flow is generated in a micro-/nano-channel by the action of an externally applied electric field on the mobile charges present in a liquid near its interface with a solid surface. A surface of homogeneous composition gives rise to the idealized case of uniform wall surface potential (or uniform

© 2013 The Japan Society of Fluid Mechanics and IOP Publishing Ltd Printed in the UK
0169-5983/13/055502+14$33.00

ζ-potential). In microchannels, these conditions lead to a flow field that is longitudinally uniform (Probstein 1994) barring entrance and exit effects. However, in actual microchannels inhomogeneities in the surface chemistry may be present either as an artifact of their fabrication process or may be deliberately engineered through surface modification technologies (Stroock *et al* 2000, Biddiss *et al* 2004) which renders the wall zeta potential (or surface charge) a variable. The motivation for engineering wall surface potential variation in microchannels is often the fact that the resultant electro-osmotic flow field contains vortices that are expected to facilitate mixing (Stroock *et al* 2000), given that mixing of reagents is usually considered to be a difficult task in microfluidics because of the absence of turbulence (Stone *et al* 2004). Axial variations of zeta potential give rise to longitudinally nonuniform flow fields that have been theoretically analyzed by several authors, e.g. by Anderson and Idol (1985), Long *et al* (1999), Herr *et al* (2000), Ghosal (2002) and Horiuchi *et al* (2007) in the limit of infinitely thin double layers and Ajdari (1996) Yariv (2004) and Khair and Squires (2008) for finite electrical double layer thickness. Yariv (2004) and Khair and Squires (2008) has studied the flow near a single surface with a surface charge discontinuity, while Ajdari (1996) has studied a two-dimensional geometry, which in today's parlance can be termed as a nanochannel. Numerical/semi-analytical studies on electro-osmotic flow with variable wall potential include Xuan and Li (2005), Datta *et al* (2006) and Chen and Conlisk (2009). Since recent enhancements in fabrication technologies (Schoch *et al* 2008) have made flows through nanochannels where the channel height is not much larger than the characteristic thickness of the electrical double layers (EDL) experimentally realizable, works such as by Ajdari (1996) where the assumption of infinitely thin EDL is not used as the starting point of theoretical analyses, are worth revisiting for generalization to situations where additional physical phenomena are also relevant.

Another characteristic of nanochannels is that the effects of hydrodynamic slippage on flow fields can be significant (Majumder *et al* 2005, Eijkel 2007, Lauga *et al* 2007, Vinogradova *et al* 2009) not only for gases (Karniadakis *et al* 2005) but even for the flow of liquids so that it is no longer appropriate to use the no slip boundary condition, standard in macroscale fluid dynamics. Further, the possible ubiquitous presence of the effects of slippage in observations of electro-osmotic flow has been acknowledged recently (Eijkel 2007, Bocquet and Charlaix 2010).

The situations dealt with in studies on liquid slippage can be broadly categorized into intrinsic or molecular slip (Joly *et al* 2004, Majumder *et al* 2005, Wang and Zhao 2011, Priezjev 2013) and 'effective slip'. Studies on 'effective slip' surmise that a single effective slip length which can characterize on a macroscopic or experimental length scale the microscopic effects of the complex surface topography, wettability characteristics, adhered gas layers etc, can be ascribed to a surface or a flow-confining geometry. The concept of effective slip is reviewed, (e.g. in Stone *et al* 2004, Lauga *et al* 2007, Squires 2008, Vinogradova and Belyaev 2011). Effective slip has been studied in pressure-driven/shear flows (Lauga and Stone 2003, Hendy and Lund 2007, Feuillebois *et al* 2009, Lund and Hendy 2009, Belyaev and Vinogradova 2010, Asmolov *et al* 2012) and/or in electrokinetic flows (Squires 2008, Bahga *et al* 2010, Zhao 2010, Belyaev and Vinogradova 2011, Ng and Chu 2011, Chu and Ng 2012, Ng and Zhou 2012a, 2012b). With the exception of Squires (2008), the studies mentioned in the last sentence also involve detailed microscopic model of the slipping/non-slipping surfaces. For calculating the effective slip of a 'microscopically' slipping surface (either due to surface-adhered gas layers or due to molecular slip), a commonly employed model for flow calculations involves alternating regions of perfect slip (zero shear stress or equivalently infinite slip length) and no slip or

'stick' on the surface as employed by Zhao (2010) and Bahga *et al* (2010). However, more recent works have also employed the more realistic partial slip (finite slip length) boundary condition (Belyaev and Vinogradova 2011, Ng and Chu 2011, Chu and Ng 2012, Ng and Zhou 2012a) on the non-sticking regions.

Most studies on 'effective slip' in electrokinetic flows explore the flow field near a single surface (Bahga *et al* 2010, Zhao 2010, Belyaev and Vinogradova 2011), in the sense that the characteristic channel width of any confining geometry is assumed to be much larger than the largest of the following three length scales: (i) the Debye length or the length scale of the electrical double layer, (ii) the microscopic slip length and (iii) the length scale of the microscopic channel surface inhomogeneities. However, the more recent work of (Ng and Chu 2011, Chu and Ng 2012, Ng and Zhou 2012a, 2012b) study confined flows without the above-discussed restriction on the relative magnitude of the length scales mentioned above. The current study also does not place the above-discussed restriction, in the sense that the analysis and results are applicable to finite electrical-double-layer-thickness to channel-width ratios, finite slip-length to channel-width ratios and finite surface-charge-variation-wavelength to channel-width ratios. It can be noted, however, that the theoretical models employed by Ng and Zhou (2012a, 2012b) are subject to the restriction (arising from the use of the lubrication approximation) that the ratio of the characteristic wavelength of surface charge variation on the channel wall be 'large' compared to the channel width.

The 'microscopic' calculations involved in obtaining the effective slip length in the above studies are either (a) numerical e.g. Zhao (2010) solves the nonlinear Poisson–Nernst–Planck equation for large surface potentials, or (b) semi-analytical in nature e.g. in order to impose the boundary condition on the velocity component tangential to the surface, dual series are solved numerically by Zhao (2010) and Bahga *et al* (2010) and point collocation on truncated series are employed by Ng and Chu (2011) and Chu and Ng (2012)), or (c) based on a perturbative approach such as the lubrication approximation e.g. Ng and Zhou (2012a) for circular channels, Ng and Zhou (2012b) for slits; the latter is the same geometry as in the current work) or the smallness of the dimensionless amplitude of surface inhomogeneity (Zhao 2012). In contrast, as demonstrated later, the problem solved in the current study is tractable in closed form (subject to the Debye–Huckel and creeping flow approximations) using exact analysis rather than numerical/semi-analytical tools and the corresponding results are valid for any ratio of surface-charge-variation wavelength to channel height, unlike results from lubrication theory.

The current study is conducted with the more realistic partial slip rather than the perfect slip approximation; however, unlike above-discussed works, the current study does not intend to calculate the 'effective slip length and therefore, does not ascribe any pattern or distribution to the 'microscopic' slip length. Rather, the problem is formulated and solved in such a way that the results can demonstrate the effect of the degree of slippage (represented by a spatially homogeneous slip length) on the flow patterns (such as the the recirculation rolls earlier reported in channels with non-slipping walls by Ajdari (1996)) and velocity field arising from a spatially inhomogeneous surface charge density. The results also highlight an important but scarcely reported aspect by which the resultant axially inhomogeneous flow field differs in terms of the effect of slip from its spatially homogeneous counterpart which arises from uniformly charged walls, especially in the thin double layer limit.

A common physical model in the literature on 'effective slip' in electrokinetic flows, as discussed above, involves assuming that the local slip and the local surface charge are correlated to each other. In the current study, unlike the electrokinetic slippage studies discussed in the last few paragraphs (with the exception of Ng and Zhou (2012a), a

study conducted on electrokinetic flow and solute transport in circular channels), the wavelength characterizing the surface charge variation and the degree of slippage are kept as independently controllable parameters throughout the analysis and the discussion of results. Although the calculation of effective slip is not the primary objective of this work and the combination of unpatterned slip and patterned surface charge may not be an easily realizable experimental situation, the authors believe that the insight from studying the canonical problem set up in the current work can also be useful to a future study involving slip patterning.

The current study also intends to compare the exact analytical results for arbitrary wavelength of surface charge variation with that of the simpler and physically insightful lubrication approach, which is formally applicable only to surface charge patterns with wavelengths much longer than the channel width. This comparison will also give an idea of the numerical values of the wavelengths above which the lubrication approach ceases to be appropriate. To that end, the lubrication theory for Stokes flow has been presented in the appendix using a formalism (Van Dyke 1987) slightly different from Ng and Zhou (2012a, (2012b). One advantage of this formalism is that certain intermediate theoretical results (equations (A.1)–(A.4)) can be readily used to generalize the theory to higher orders in the wave-number i.e. shorter wavelengths), if required by a future study. To the knowledge of the authors, the above-discussed comparison is currently unavailable in the literature.

The purpose of this work is to study the effect of hydrodynamic slip on the electro-osmotic flow field in a nanochannel with thick EDL under a periodically patterned wall surface potential. The four important length scales in this problem are the electrical double layer length scale ('Debye length'), the cross-dimension of the channel, the wavelength of wall surface potential variations and a length scale characterizing slip. Electro-osmotic flow problems can either be analyzed by a given surface potential (Anderson and Idol 1985, Long *et al* 1999, Herr *et al* 2000, Ghosal 2002, Horiuchi *et al* 2007) or a given surface charge (Ajdari 1996, Yariv 2004) boundary condition; the former approach is adopted here. An explicit closed form analytical solution for the problem is presented. The results discuss certain interesting features of the flow field that are brought forth by the presence of slip.

2. Theoretical formulation

Consider a plane channel of height $2h$ with walls at $y = \pm h$ carrying an aqueous electrolyte solution. Let $\hat{\mathbf{i}}$ and $\hat{\mathbf{j}}$ be the unit vectors along the axial coordinate x and the cross-channel (transverse) coordinate y, respectively. The zeta potential has a periodic variation along each wall of the channel as per the law $\zeta(x) = \zeta_0 \cos(kx)$, where k is the wave number (spatial frequency) and ζ_0 is the amplitude of the periodic variation. The motivation for assuming a periodic zeta potential distribution is that, using its response more general variations can be synthesized using Fourier analysis. The resultant electric potential distribution within the channel is $\phi(x, y)$, which gives rise to a volumetric charge density ρ_e within the channel. A flow field $\mathbf{u} = u\hat{\mathbf{i}} + v\hat{\mathbf{j}}$ results from the action of a constant axial electric field $E\hat{\mathbf{i}}$ on ρ_e.

For solving the electrostatic problem in closed form, the Debye–Huckel approximation (Ajdari 1996, Yariv 2004) will be employed, which is valid if $\phi e/(kT)$ is small (Probstein 1994), where e, k and T are the electronic charge, Boltzmann's constant and absolute temperature, respectively. Under this approximation $\rho_e = -\varepsilon \nabla^2 \phi = -\varepsilon \phi / \lambda^2$, where λ is the Debye length and ε is the electrical permittivity. Further, the flow field will be studied in the limit of zero Reynolds number, an approximation appropriate for most microfluidic situations (Stone *et al* 2004). The equations of electrostatics and fluid flow, can, therefore be

written as

$$\nabla^2\phi = \frac{\phi}{\lambda^2}, \tag{1}$$

$$\mu\nabla^2\mathbf{u} - \nabla p - \varepsilon\frac{\phi}{\lambda^2}E\hat{\mathbf{i}} = 0, \tag{2}$$

$$\nabla\cdot\mathbf{u} = 0, \tag{3}$$

which are to be solved with the following boundary conditions:

$$\phi|_{y=h} = \zeta_0\cos(kx), \tag{4}$$

$$\left.\frac{\partial\phi}{\partial y}\right|_{y=0} = 0, \tag{5}$$

$$\left.\left(b\frac{\partial u}{\partial y} + u\right)\right|_{y=h} = 0, \tag{6}$$

$$v|_{y=h} = 0, \tag{7}$$

$$\left.\frac{\partial u}{\partial y}\right|_{y=0} = 0, \tag{8}$$

$$v|_{y=0} = 0. \tag{9}$$

Here, μ is the viscosity and p is the pressure modified by an additive constant $-\varepsilon\kappa^2\phi$ representing the Maxwell stresses in the equilibrium EDL (Ajdari 1995). In equations (1)–(3) and henceforth, all vector operators should be interpreted to be two-dimensional, i.e. defined on the x–y plane. Equation (6) imposes the 'Navier slip' boundary condition, wherein the parameter b is the slip length (Lauga *et al* 2007). In nanochannel flows, b can be comparable to the other length-scales in the problem viz. the geometric length scale h and the electrostatic scale λ, particularly if hydrophobic surfaces are employed (Eijkel 2007, Lauga *et al* 2007, Vinogradova *et al* 2009). Equations (8) and (9) follow from the symmetry of the problem.

For non-dimensionalization, the scales h for x and y, ζ_0 for ϕ, the Helmholtz–Smoluchowski scale $u_0 = -\frac{\varepsilon\zeta_0 E}{\mu}$ for $\mathbf{u}$ and the scale $\mu u_0/h$ for pressure are introduced. The notation for the corresponding dimensionless variables are X, Y, Φ, $\mathbf{U} = U\hat{\mathbf{i}} + V\hat{\mathbf{j}}$ and P, respectively. Further, here onward all differential operators should be interpreted to be non-dimensionalized versions, rendered dimensionless by the scale h for x and y (e.g. $\nabla \leftarrow \nabla/h$ and $\nabla^2 \leftarrow \nabla^2/h^2$), although no change in notation is introduced. The dimensionless equations take the following form (equations (10)–(12)):

$$\nabla^2\Phi = \kappa^2\Phi, \tag{10}$$

$$\nabla^2\mathbf{U} - \nabla P + \kappa^2\Phi\hat{\mathbf{i}} = 0, \tag{11}$$

$$\nabla\cdot\mathbf{U} = 0. \tag{12}$$

Here, κ is a dimensionless number given by h/λ. The boundary conditions given by equations (4)–(9) take the following dimensionless form (equations (13)–(18)):

$$\Phi|_{Y=1} = \cos(KX), \tag{13}$$

$$\left.\frac{\partial\Phi}{\partial Y}\right|_{y=0} = 0, \tag{14}$$

$$\left(B\frac{\partial U}{\partial Y}+U\right)\Bigg|_{Y=1}=0, \tag{15}$$

$$V|_{Y=1}=0, \tag{16}$$

$$\left.\frac{\partial U}{\partial Y}\right|_{y=0}=0, \tag{17}$$

$$V|_{Y=0}=0. \tag{18}$$

Here, $B=b/h$ is the dimensionless slip length and $K=kh$ is the dimensionless wave number.

Equation (10) can readily solved with its boundary conditions (equations (13) and (14)) using the separation of variables technique to give equation (19).

$$\Phi=\frac{\cosh(Qy)}{\cosh(Q)}\cos(KX), \tag{19}$$

where $Q=\sqrt{\kappa^2+K^2}$.

To solve for the flow field, an approach (see e.g. Leal 1992) is adopted, wherein the momentum and continuity equations (equations (11) and (12)) are converted into a single equation (equation (20)) for the streamfunction ψ defined by $U=\dfrac{\partial\psi}{\partial Y}$ and $V=-\dfrac{\partial\psi}{\partial X}$, after elimination of pressure (P). After rewriting the boundary conditions (equations (15) and (16)) in terms of ψ, the following problem for ψ (equations (20)–(24)) is obtained:

$$\nabla^4\psi=-\kappa^2\frac{\partial\Phi}{\partial Y}, \tag{20}$$

$$\left.B\frac{\partial^2\psi}{\partial Y^2}+\frac{\partial\psi}{\partial Y}\right|_{Y=1}=0, \tag{21}$$

$$\left.\frac{\partial\psi}{\partial X}\right|_{Y=1}=0, \tag{22}$$

$$\left.\frac{\partial^2\psi}{\partial Y^2}\right|_{Y=0}=0, \tag{23}$$

$$\left.\frac{\partial\psi}{\partial X}\right|_{Y=0}=0. \tag{24}$$

Here, $\nabla^4=\frac{\partial^4}{\partial X^4}+2\frac{\partial^2}{\partial X^2}\frac{\partial^2}{\partial Y^2}+\frac{\partial^4}{\partial Y^4}$ is the biharmonic differential operator. Note that, on differentiating equation (19), $\dfrac{\partial\Phi}{\partial Y}=\dfrac{Q\sinh(QY)}{\cosh(Q)}\cos(KX)$ may be substituted in the term on the right hand side of equation (20).

A solution of the form $f(y)\cos(KX)$ will satisfy equations (20)–(24) provided $f(y)$ is given by:

$$f(y) = A_1 \sinh(KY) + A_2 Y \cosh(KY) - \frac{Q \sinh(QY)}{\kappa^2 \cosh(Q)}, \tag{25}$$

where

$$A_1 = \frac{Q\cosh(K)\left[\tanh(Q)\left(1 - B\kappa^2\right) - Q\right] + kQ\sinh(K)\tanh(Q)(2B+1)}{\kappa^2\left(\cosh(K)\sinh(K) + BK\cosh(2K) - (B+1)K\right)}, \tag{26}$$

$$A_2 = \frac{Q\left[Q\sinh(K) + \tanh(Q)\left(B\kappa^2\sinh(K) - K\cosh(K)\right)\right]}{\kappa^2\left(\cosh(K)\sinh(K) + BK\cosh(2K) - (B+1)K\right)}. \tag{27}$$

Equations (25) with equations (26) and (27) are the key results of the analysis and can be used to study the effect of slippage on electro-osmotic flow patterns. As suggested by Ajdari (1996) in the context of non-slipping flows, a related flow pattern having the (dimensionless) form $\psi' = f'(Y)\cos(KX)$ corresponds to the situation the periodic variation on the bottom wall lags the $\zeta\cos(kx)$ pattern on the top wall by a phase angle of π. The corresponding $f'(y)$ is given by

$$f'(y) = A_1' \cosh(KY) + A_2' Y \sinh(KY) - \frac{Q\cosh(QY)}{\kappa^2\sinh(Q)}, \tag{28}$$

where

$$A'_1 = \frac{kQ\cosh(K)\coth(Q)(2B+1) - Q\sinh(K)\left[\coth(Q)\left(B\kappa^2 - 1\right) + Q\right]}{\kappa^2\left(\cosh(K)\sinh(K) + Bk\cosh(2K) + (B+1)K\right)}, \tag{29}$$

$$A_2 = \frac{Q\left[Q\cosh(K) + \coth(Q)\left(B\kappa^2\cosh(K) - K\sinh(K)\right)\right]}{\kappa^2\left(\cosh(K)\sinh(K) + BK\cosh(2K) + (B+1)K\right)}. \tag{30}$$

Then, the more general case of the bottom wall lagging the top wall by an arbitrary angle θ can be worked out through the linear superposition $\cos(\theta/2)\psi - \sin(\theta/2)\psi'$.

3. Results and discussion

The flow field, given by $U = f_1(Y)\cos(KX)$ and $V = Kf(Y)\sin(KX)$ has the characteristic that there is no net flow through the channel cross-section. Similar to the case with no slip (Ajdari 1996), the streamlines shown in figure 1 form closed loops that indicate four counter-rotating vortices per periodic cell forming the flow field. It is interesting to investigate the U profile at $X = 0$ (where $V = 0$) and V profile at $X = \pi/(2K)$ (where $U = 0$), in order to study the effect of slip. The first axial location will house the global maxima/ minima in U, while the second axial location will house the global maxima/minima in V. In figure 1, the location $X = \pi/(2K)$ is indicated with a dark line.

Figure 2 studies the effect of increasing B on $U(0, Y)$ for $\kappa = 5$ and $K = 1$. There are, in general three extrema in U which include a minimum at the centerline of the channel and two local maxima closer to the wall. As the degree of slip given by the magnitude of B is increased, the minimum velocity increases in magnitude; the maxima shift toward the walls, while also increasing in magnitude. The near-wall side of the maxima also become 'gentler'(less steep) with increasing B. For large B the maxima appears on the wall. With increasing slippage, the zone of reversed flow near the center of the channel increases in size.

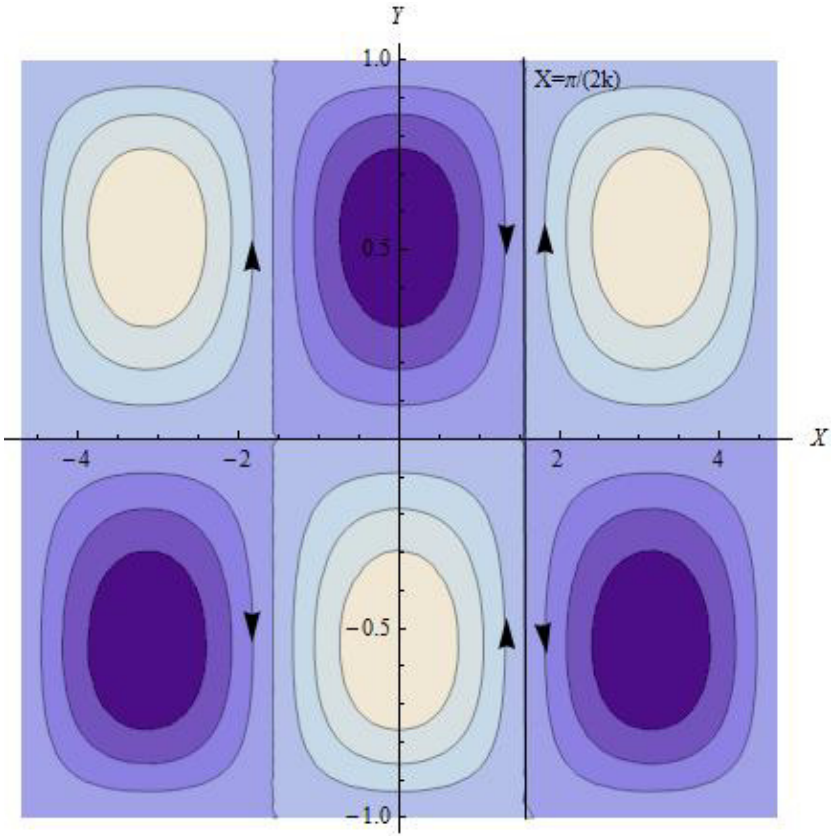


Figure 1. The streamlines of flow for $B = 1$, $\kappa = 5$ and $K = 1$ shown for $-3\pi/(2K) < X < 3\pi/(2K)$.

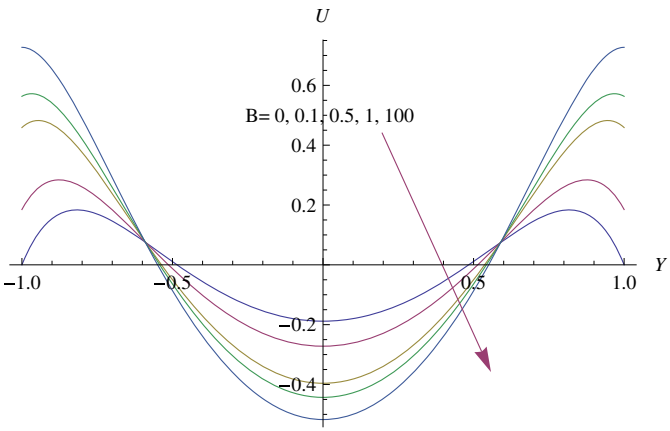


Figure 2. Variation across the channel of the axial velocity component U at $X = 0$ with slip length for $\kappa = 5$ and $K = 1$.

It is interesting to note that having a large B ($B = 100$ in figure 2) does not lead to large U velocity magnitudes in figure 2; rather, the effect of B in increasing the magnitudes of the velocity extrema tends to saturate, ultimately approaching the solution of the theoretical

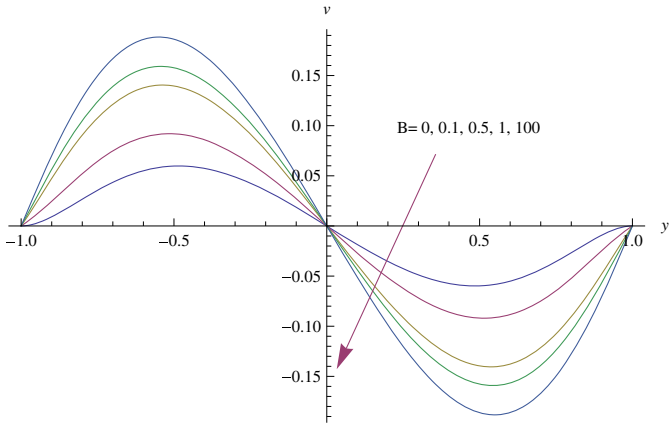


Figure 3. Variation across the channel of cross-channel velocity component V at $X = \pi/(2K)$ with slip length for $\kappa = 5$ and $K = 1$.

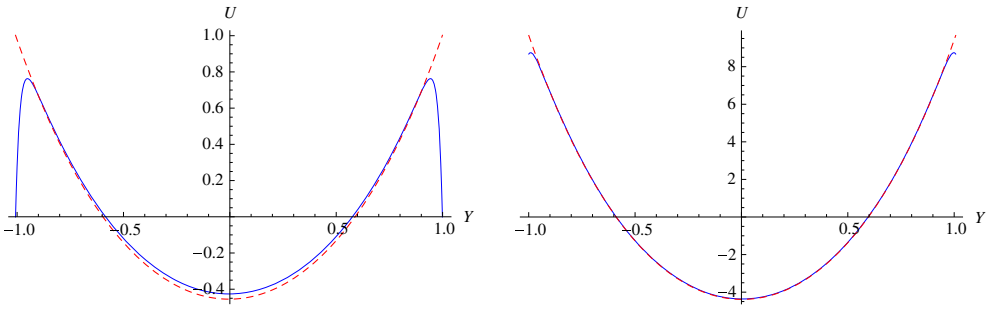


Figure 4. $U(0, Y)$ profiles for large κ ($\kappa = 50$). Left and right panes are for $B = 0$ and 0.5, respectively. The dashed lines on both panes are predictions from an apparent Helmholtz–Smoluchowski apparent slip boundary condition based approach discussed in the text.

model in the limit of 'perfect slip' as B is increased; in fact, the profile for $B = 1$ is not very dissimilar from that for $B = 100$. This result is in contrast to that for a purely electro-osmotic flow with uniform wall surface potential and slipping walls, for which it can be deduced easily from the fully-developed form of equations (10)–(12) and equations (4)–(9):

$$U(Y) = 1 - \frac{\cosh(\kappa Y)}{\cosh(\kappa)} + B\kappa \tanh(\kappa), \tag{31}$$

indicating that the velocity magnitude at a given Y (and the flow rate) can increase out of bounds for large B. Figure 3 shows the variation of the V profiles at $X = \pi/(2K)$ with slip for $\kappa = 5$ and $K = 1$. In this case also, slip enhances the magnitude of the extrema, with the extrema nearest to the walls shifting slightly closer to the walls as slip increases.

Figure 4 studies the limit of thin electric double layers (large κ). The $U(0, y)$ profile at $X = 0$ for the no slip case ($B = 0$) shown on the left pane reveals steep drops localized in the near-wall zone. The U in the core region of the channel is well-reproduced by a theory (dashed line on the left pane) based on the application of the so-called Helmholtz–Smoluchowski apparent slip boundary condition (Anderson and Idol 1985, Ajdari 1996) to the core body-force-free flow to represent the effect of EDL. In the parlance of the current analysis,

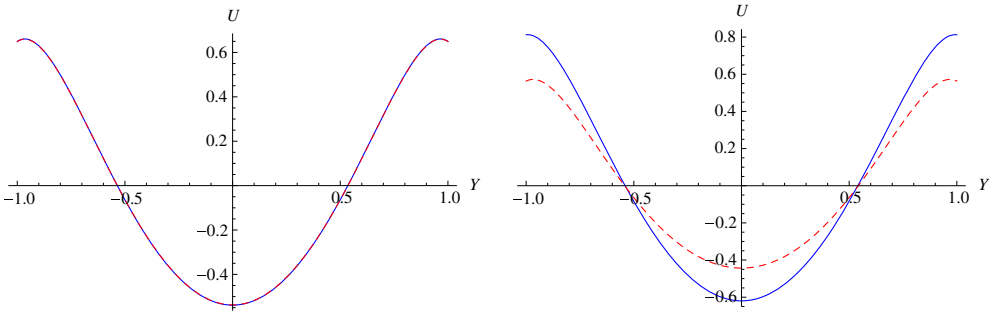


Figure 5. $U(0, Y)$ profiles (solid lines) for $\kappa = 5$ and $B = 1$ compared with the lubrication limit result based on equation (A.9) (dashed lines) for $K = 0.1$ (left pane) and for $K = 1$ (right pane).

this theory corresponds to (a) replacing the boundary condition $U(X, 1) = 0$ by $U(X, 1) = \cos(KX)$ and (b) setting the right hand side of equation (20) to zero. The latter amounts to neglecting the body forces outside the EDL (in the core region). Such a theory is customarily used in the study of microchannel flows (see e.g. Anderson and Idol (1985)).

The right pane of figure 4 studies a situation with slippage ($B = 0.5$) in the limit of thin electric double layers. A Helmholtz–Smoluchowski apparent slip boundary condition for this flow field can be developed by evaluating the streamfunction calculated in the previous section in the limit of $\kappa \to \infty$ (keeping $B\kappa \sim O(1)$ at most) and finding the corresponding value of $U(X, 1)$. This gives

$$U(X, 1) = \frac{1 + B\kappa}{1 + Bg(K)} \cos(KX), \tag{32}$$

where $g(K) = \frac{2K \sinh^2(K)}{\cosh(K) \sinh(K) - K}$. The function $g(K)$ increases with K, with a small and large K behavior of $g(K) \sim 3$ and $g(K) \sim 2K$, respectively. In the small K limit, the corresponding form of equation (32) can also be predicted from the lubrication-approximation-based approach discussed in the appendix. As seen from the right pane of figure 4, the $U(0, Y)$ profile outside the thin EDLs is accurately represented by the aforesaid theory (shown by dashed lines). Equation (32) contrasts with the more well-known form for uniform zeta potential (see Belyaev and Vinogradova (2011) and the references therein; see also equation (31)), which is simply $U(X, 1) = (1 + B\kappa)\cos(KX)$. The latter is affected only by the ratio of slip length to the Debye length.

In accordance with other studies on electro-osmotic flow (e.g. Eijkel 2007), it was found that very large U and V can be generated for $\kappa \gg 1$ (i.e. in the thin double layer limit). It should be noted however, the velocity scale $\varepsilon\zeta E/\mu$ used in this study, itself, has a certain variation with electrical double layer thickness and channel height, which is beyond the scope of this study. So, care should be taken to extrapolate conclusions such as the above to the dimensional velocity. The low K behavior could be interpreted both qualitatively and quantitatively in the framework of lubrication approximation (Van Dyke 1987, Ghosal 2002). The lubrication theory with slippage is derived in the appendix and its main result is equation (A.9). According to the lubrication theory, the axial flow velocity at any given cross-section is a superposition of an electro-osmotic component and a pressure-driven component. Since the lubrication theory is formally valid in the limit $K \to 0$, it can be observed in figure 5, that the $U(0, Y)$ profile for $K = 0.1$ shown in the left pane is more accurately represented by the lubrication limit solution (equation (A.9)) than that for $K = 1$. This

is because, the lubrication-theory representation of axial component of the viscous force and the axial variation of the electric potential is not accurate when K is $O(1)$. For large κ the B dependence of the electro-osmotic component in equation (A.9) (shown in curly brackets) can be collapsed into the parameter $B\kappa$. However, the effect of slip on the pressure-driven component cannot be collapsed into that of the parameter $B\kappa$. This is because the pressure-driven flow component (with slippage) per unit induced pressure gradient is of non-electrostatic origin. This provides another insight into why the Helmholtz–Smoluchowski slip boundary condition for the spatially inhomogeneous electro-osmotic flow, viz. equation (32), has a form different from that for spatially homogeneous electro-osmotic flow (Belyaev and Vinogradova 2011).

The vortices weaken and localize near the walls for large K. It was found from the streamlines obtained using the approach discussed at the end of section 2, that on increasing the phase difference θ between the two wall patterns $\zeta\cos(kx \pm \theta/2)$ at $y = \pm h$, the system transitions from a system with two vortices across the channel width to a system with only a single vortex and that the presence of slip causes the transition to occur at a lower value of θ.

4. Conclusions

The effect of hydrodynamic slip on axially variable electro-osmotic flow generated by wall zeta potential variation, when both the slip length and the electrical double layer thickness are comparable to the nanochannel height, has been studied in this work. Equation (25) with equations (26) and (27) are the key results of the analysis carried out in the Stokes flow limit based on the Debye–Huckel approximation. An analysis for the situation when the wavelength of axial variation is much larger than the channel half-height has also been conducted on the basis of lubrication theory.

There is no net flow through a given channel cross-section. The flow consists of axially adjacent periodic cells. Each periodic cell of the flow field consists of four counter-rotating vortices. The cross-channel profile of the axial velocity at the center of the cell exhibits three extrema and a reversed velocity zone near the channel axis of symmetry. The size of the extrema and that of the reversed velocity zone increases with increase in the degree of slippage. The cross-channel profile of the transverse velocity at the edges of the periodic cell exhibit two extrema which increase in magnitude with increase in the degree of slippage.

In the limit when the wavelength of axial variation in wall surface potential is much larger than the channel width, the lubrication approximation can be used to interpret the axial velocity at any given cross-section as a superposition of an electro-osmotic flow component and a pressure-driven component driven by pressure gradients induced by the axial wall surface potential variation. However, the lubrication approach do not represent axial component of the viscous force and the axial variation of the electric potential accurately enough to be applied for wavelengths which are of the order of channel width.

In general, it can be concluded that hydrodynamic slip enhances the velocity magnitudes of the recirculating flow in response to a periodic zeta potential on the wall. However, for thick double layers, as the ratio of the slip length to channel width increases, the velocity magnitude at any given location within the channel remains bounded. For electric double layers that are much thinner than the channel width, large velocity magnitudes (scaled with $-\varepsilon\zeta E/\mu$) can be realized. To study this limit, a Helmholtz–Smoluchowski boundary condition for slipping electro-osmotic flows under patterned zeta potential has been developed. Compared to non-slipping electro-osmotic flows, the Helmholtz–Smoluchowski slip velocity is enhanced in magnitude due to hydrodynamic slippage by a factor which depends on the ratios of the slip length to Debye length, pattern wavelength and channel height. It can be noted that the

corresponding factor (see e.g. Belyaev and Vinogradova 2011) for electro-osmotic flow with unpatterned zeta potential depends only on the ratio of slip length to Debye length.

The analysis presented here can be easily generalized to more realistic zeta potential distributions, such as the square wave (Stroock *et al* 2000) through Fourier analysis. A more detailed study of the flow circulation patterns resulting from a phase difference between the periodic patterns on the walls could also be conducted, either using the approach outlined at the end of section 2 or by reformulating the problem. Future work may be directed to the related problem where the slip length varies axially. Also, the Debye–Huckel approximation may be relaxed, which will necessitate a numerical solution.

Acknowledgments

The authors are grateful for financial support from the Planning Unit, IIT Delhi. Helpful suggestions during the preparation of the manuscript from Professor Sanjeev Jain, Department of Mechanical Engineering, IIT Delhi are acknowledged.

Appendix

The flow field in the limit $K \to 0$ can be understood in terms of the lubrication approximation (Ghosal 2002). We introduce the re-scaled variables (Van Dyke 1987), $\xi = KX$, $P' = P/K$ and $V' = KV$ and rewrite equations (10)–(12) in scalar form as:

$$K^2 \frac{\partial^2 \Phi}{\partial \xi^2} + \frac{\partial^2 \Phi}{\partial Y^2} = \kappa^2 \Phi, \tag{A.1}$$

$$K^2 \left(\frac{\partial^2 U}{\partial \xi^2} + \frac{\partial^2 \Phi}{\partial \xi^2} \right) + \frac{\partial^2 U}{\partial Y^2} + \frac{\partial^2 \Phi}{\partial Y^2} = \frac{\partial P'}{\partial \xi}, \tag{A.2}$$

$$K^4 \frac{\partial^2 V'}{\partial \xi^2} + K^2 \frac{\partial^2 V'}{\partial Y^2} = \frac{\partial P'}{\partial Y}, \tag{A.3}$$

$$\frac{\partial U}{\partial \xi} + \frac{\partial V'}{\partial Y} = 0, \tag{A.4}$$

which are to be solved with the boundary conditions equations (15)–(18) and

$$\Phi|_{Y=1} = \cos \xi. \tag{A.5}$$

Note that the representation $\nabla^2 \Phi \hat{\mathbf{i}}$ of the electrical body force rather than the $\kappa^2 \Phi \hat{\mathbf{i}}$ used in equation (11) has been utilized in equation (A.2). The latter representation utilizes the Debye–Huckel approximation, whereas the former does not. The leading order solution is obtained by setting $K = 0$ in the above equations. In this limit the solution of equation (A.1) with equation (A.5) becomes

$$\Phi = \frac{\cosh(\kappa Y)}{\cosh(\kappa)} \cos \xi. \tag{A.6}$$

The solution of equation (A.2) with equations (15) and (17) is

$$U = -\frac{\mathrm{d}P'}{\mathrm{d}\xi} \left(\frac{1 - Y^2}{2} + B \right) + \Phi(\xi, 1) - \Phi(\xi, Y) + B \left. \frac{\partial \Phi}{\partial Y} \right|_{Y=1}. \tag{A.7}$$

Equation (A.4) can be combined with equation (16) and (18) to conclude that $\frac{dQ}{dx} = 0$ where $Q = 2\int_0^1 U dy$ is the volume flow rate (per unit depth) through the channel.

The volume flow rate Q may also be evaluated by integrating equation (A.7) between $y = 0$ and 1. On rearrangement of the resultant equation, the following expression for $\frac{dP'}{d\xi}$ is obtained

$$\frac{dP'}{d\xi} = \frac{2\left(\Phi(\xi, 1) - \bar{\Phi} + B\left.\frac{\partial \Phi}{\partial Y}\right|_{Y=1}\right) - Q}{2\left(B + \frac{1}{3}\right)}, \tag{A.8}$$

where $\bar{\Phi} = \int_0^1 \Phi \ dy$ is the cross-channel average of Φ. Equation (A.8) can be integrated over one periodic cell i.e between $\xi = -\pi$ to π. Since there is no imposed pressure $P(\xi = \pi) = P(\xi = -\pi)$, because of equation (A.6), the integral of the second, third and fourth terms in equation (A.8) are zero over a periodic cell. Therefore, $Q = 0$, i.e. there is no net flow through the channel. Setting $Q = 0$ in equation (A.8) and substituting the resultant expression for $\frac{dP'}{d\xi}$ in equation (A.7), the following result is obtained:

$$U = \cos(KX)\left[\left\{1 - \frac{\cosh(\kappa Y)}{\cosh(\kappa)} + B\kappa \tanh(\kappa)\right\} - \frac{3}{3B+1}\left(1 - \frac{\tanh(\kappa)}{\kappa} + B\kappa \tanh(\kappa)\right)\left(\frac{1 - Y^2}{2} + B\right)\right]. \tag{A.9}$$

In the above equation, equation (A.6) has been utilized. The term in curly brackets signifies an electro-osmotic flow component and the remainder of the terms signify a pressure-driven flow due to the induced pressure-gradients set up due to the wall surface potential variation.

References

Ajdari A 1995 *Phys. Rev. Lett.* **75** 755–8
Ajdari A 1996 *Phys. Rev.* E **53** 4996
Anderson J and Idol W 1985 *Chem. Eng. Commun.* **38** 93–106
Asmolov E S, Zhou J, Schmid F and Vinogradova O I 2012 arXiv:1212.6127
Bahga S S, Vinogradova O I and Bazant M J 2010 *J. Fluid Mech.* **644** 245–55
Belyaev A V and Vinogradova O I 2010 *J. Fluid Mech.* **652** 489
Belyaev A V and Vinogradova O I 2011 *Phys. Rev. Lett.* **107** 098301
Biddiss E, Erickson D and Li D 2004 *Anal. Chem.* **76** 3208–13
Bocquet L and Charlaix E 2010 *Chem. Soc. Rev.* **39** 1073–95
Chen L and Conlisk A 2009 *Biomed. Microdevices* **11** 251–8
Chu H C W and Ng C O 2012 *ASME J. Fluids Eng.* **134** 11201
Datta S, Ghosal S and Patankar N 2006 *Electrophoresis* **27** 611–9
Eijkel J 2007 *Lab Chip* **7** 299–301
Feuillebois F, Bazant M Z and Vinogradova O I 2009 *Phys. Rev. Lett.* **102** 026001
Ghosal S 2002 *J. Fluid Mech.* **459** 103–28
Hendy S C and Lund N J 2007 *Phys. Rev.* E **76** 066313
Herr A, Molho J, Santiago J, Mungal M, Kenny T and Garguilo M 2000 *Anal. Chem.* **72** 1053–7
Horiuchi K, Dutta P and Ivory C 2007 *AIChE J.* **53** 2521–33
Joly L, Ybert C, Trizac E and Bocquet L 2004 *Phys. Rev. Lett.* **93** 257805
Karniadakis G, Beskok A and Aluru N 2005 *Microflows and Nanoflows* (New York: Springer)
Khair A S and Squires T M 2008 *J. Fluid Mech.* **615** 323–4
Lauga E, Brenner M and Stone H A 2007 *Handbook of Experimental Fluid Mechanics* ed C Tropea, A Yarin and J F Fouss (New York: Springer) chapter 19, pp 1219–40
Lauga E and Stone H A 2003 *J. Fluid Mech.* **489** 55–77
Leal L 1992 *Laminar Flow and Convective Transport Processes: Scaling Principles and Asymptotic Analysis* (Boston, MA: Butterworth-Heinemann)

Long D, Stone H and Ajdari A 1999 *J. Colloid Interface Sci.* **212** 338–49
Lund N J and Hendy S C 2009 *Aust. New Zealand Indust. Appl. Math. J.* **50** 381–94
Majumder M, Chopra N, Andrews R and Hinds B 2005 *Nature* **438** 44
Ng C O and Chu H C W 2011 *Phys. Fluids* **23** 102002
Ng C O and Zhou Q 2012a *Phys. Fluids* **24** 112002
Ng C O and Zhou Q 2012b *Fluid Dyn. Res.* **44** 055507
Priezjev N V 2013 *Microfluids Nanofluids* **14** 225–33
Probstein R 1994 *Physicochemical Hydrodynamics* (New York: Wiley)
Schoch R, Han J and Renaud P 2008 *Rev. Mod. Phys.* **80** 839
Squires T M 2008 *Phys. Fluids* **20** 092105
Stone H, Stroock A and Ajdari A 2004 *Annu. Rev. Fluid Mech.* **36** 381–411
Stroock A, Weck M, Chiu D, Huck W, Kenis P, Ismagilov R and Whitesides G 2000 *Phys. Rev. Lett.* **8415** 3314–7
Van Dyke M 1987 *Adv. Appl. Mech.* **25** 1–45
Vinogradova O I and Belyaev A V 2011 *J. Phys.: Condens. Matter* **23** 184104
Vinogradova O, Koynov K, Best A and Feuillebois F 2009 *Phys. Rev. Lett.* **102** 118302
Wang F C and Zhao Y P 2011 *Soft Matter* **7** 8628–34
Xuan X and Li D 2005 *J. Colloid Interface Sci.* **289** 291–303
Yariv E 2004 *J. Fluid Mech.* **521** 181–9
Zhao H 2010 *Phys. Rev.* E **81** 066314
Zhao C and Yang C 2012 *Electrophoresis* **33** 899–905